


Robust broken-gap MoTe₂/ZrS₂ van der Waals heterostructureS. Samaneh Ataei and Ali Sadeghi ^{*}*Department of Physics, Shahid Beheshti University, 1983969411, Tehran, Iran*

(Received 19 May 2022; revised 17 November 2022; accepted 21 November 2022; published 5 December 2022)

Two-dimensional van der Waals (vdW) heterostructures with several possibilities of band edge alignment are promising candidates in the design of semiconductor junction devices with good electrostatic control. We predict a robust broken-gap band alignment for the MoTe₂/ZrS₂ vdW heterostructure and uncover the underlying mechanism. Our first-principles calculations reveal that upon formation of the vdW heterostructure a small amount of charge is transferred between the layers which sits on the central transition metal atoms and is responsible for the band edge alignment. Moreover, the lattice-mismatch-induced in-plane strain and the interfacial polarization are shown to play no role in band alignment. However, we find a weak sensitivity of the electronic structure and band edge alignment of the vdW heterostructures to an external normal-to-plane strain or electric field. Our findings are helpful in designing heterojunction devices with desired electronic structures.

DOI: [10.1103/PhysRevB.106.245301](https://doi.org/10.1103/PhysRevB.106.245301)**I. INTRODUCTION**

Heterostructures offer unique degrees of freedom in the design of semiconductor junction devices. For example, two-dimensional (2D) semiconductor-based heterojunction solar cells with the spatial separation of photogenerated electron-hole pairs show enhanced power-conversion efficiency [1]. The large controllability of the conduction and valence band offsets at the junction makes heterostructures suitable for various optoelectronic applications. For two semiconductors in contact, three types of band edge alignment are possible [2]. In the so-called *straddling* (or type I) and *staggered* (or type II) lineups, there is no overlap between the valence and conduction bands of the heterostructure. Most studies on van der Waals (vdW) layered heterostructures with different stacking of the layers demonstrate a staggered-gap semiconductor [3–6]. On the other hand, in the less-studied *broken-gap* (or type III) band alignment [7–9], the bottom of the conduction band of one semiconductor drops below the top of the valence band of the other one. This closed-gap exotic situation not only is of research interest but also has potential practical applications in tunnel field-effect transistors (TFETs) [10,11].

Transition metal dichalcogenide (TMD) heterostructures with reduced screening and weak vdW interlayer interactions have recently attracted great attention for optoelectronic applications [12–16]. Mechanical strain [17,18] or external electric field [19] is applied to tune the optoelectronic properties [20,21] and control the tunneling probability and thus the “on-current”-to-“off-current” ratio hence enhancing the performance of the heterostructure TFETs [22]. Compared with the conventional field-effect transistors, TFETs suffer from the very small tunneling probability and hence “on-current.” The tunneling probability can be enhanced in

two-dimensional TFETs thanks to the possibility of applying high electric fields at the junction. Moreover, atomistic simulations revealed a high performance for TMD TFETs enabled by increasing the tunneling probability via adapting electronic properties such as the band gap and effective mass by the choice of the TMDs [23]. In this context, stacked layers with similar lattice properties are preferred for designing TMD heterostructures with broken-gap band alignment for TFET applications, so that variability reduction by adopting heterostructures based on MoTe₂/SnS₂, MoTe₂/ZrS₂, or HfS₂/SnSe₂ has been proposed [11].

In this paper, we present an in-depth study of the electronic structure of the MoTe₂/ZrS₂ vdW heterostructure. Our first-principles calculations show a broken-gap band alignment for this heterostructure and reveal that the responsible mechanism is the charge transfer into the transition metal (TM) atoms. The interfacial polarization and the lattice-mismatch-induced strain are shown to have a marginal effect on the band alignment of the heterostructure. Furthermore, we study the effect of external normal-to-plane strain and electric field and show that a transition to the staggered gap occurs at extremely large fields. In the rest of this paper, the detailed results are presented and discussed following the introduction of our computational methodology.

II. COMPUTATIONAL DETAILS

The first-principles calculations are performed in the framework of density functional theory (DFT) within the Perdew-Burke-Ernzerhof (PBE) approximation of the exchange-correlation functional [24] as implemented in the QUANTUM ESPRESSO code package [25]. To obtain numerically well converged results, the valence electron wave function is expanded in terms of a plane-wave basis set with a kinetic energy up to 100 Ry while the irreducible Brillouin zone is sampled on a $18 \times 18 k$ grid. Fully relativistic norm-conserving pseudopotentials [26] are employed to

^{*}ali_sadeghi@sbu.ac.ir

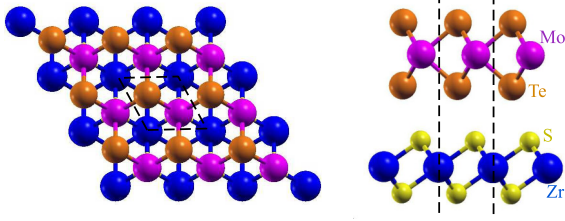


FIG. 1. Top and side views of the $2H$ - $\text{MoTe}_2/1T$ - ZrS_2 heterostructure used in our computations. The dashed lines outline one unit cell.

represent the core states by taking into account the spin-orbit interactions. The energy convergence criterion for wavefunction optimization is set to 2 meV. To determine the relaxed configurations, atomic nuclei are iteratively relaxed until the maximum force component on each atom becomes smaller than $0.01 \text{ eV}/\text{\AA}$. The supercell method with a vacuum gap of height about 18 \AA is used to prevent spurious interaction between periodic images of the heterostructure. A normal-to-plane strain is introduced by rigidly moving one layer with respect to the other without rereleasing the atoms. When an external electric field is applied normal to the layer plane, a correction dipole layer is introduced in the vacuum [27,28] while a jellium model (homogeneous background charge) is used for neutralizing the supercell of doped systems. The vacuum level is the energy reference in the band structure diagrams. In a textbook picture, the vacuum level is the electrostatic potential far away from the sample surface [29]. Similarly, we set the energy of the vacuum level to be the same as the electrostatic potential in the middle of the vacuum region (for details, see Supplemental Material [30], where we also explain how the contribution from the uniform external electric field or the homogeneous background charge is first eliminated from the electrostatic potential).

Our calculated lattice constants of the monolayers $2H$ - MoTe_2 and $1T$ - ZrS_2 are 3.53 and 3.64 \AA , respectively, in good agreement with experiment (3.52 and 3.66 \AA) and previous computations with the optB86b functional (3.53 and 3.65 \AA) [31]. Among six possible highly symmetric conformations achievable by stacking the two monolayers [9], we address the stacking of unrotated single unit cells of MoTe_2 and ZrS_2 , as depicted in Fig. 1. There is a lattice mismatch of about 3% between the two monolayers. We thus initially set the common lattice constant of the layers in the heterostructure equal to the mean of those of the isolated layers and then minimize the total energy of the $\text{MoTe}_2/\text{ZrS}_2$ heterostructure with respect to the in-plane lattice constant, which results in an optimized common lattice constant of 3.59 \AA . When the vdW interactions between the monolayers are introduced by the Grimme approximation method [32], the formation energy of the heterostructure (i.e., the energy required to separate the two constituting monolayers) is calculated to be 0.198 eV per cell while the equilibrium interlayer separation is 3.13 \AA . With the rev-vdW-DF2 functional [33] (which is also expected to predict accurately the equilibrium geometries of the layered structures [34]), the equilibrium interlayer separation is 3.01 \AA .

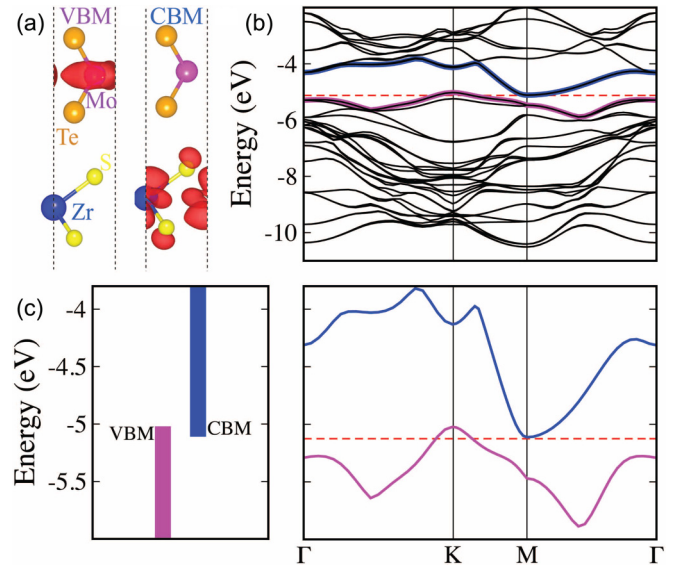


FIG. 2. (a) Spatial distribution of the highest occupied and lowest unoccupied orbitals and (b) band structure of $\text{MoTe}_2/\text{ZrS}_2$ vdW heterostructure. The valence and conduction bands are indicated in magenta and blue, their edges (VBM and CBM) occur at the K and M points, and the corresponding orbitals in (a) are mainly localized on the Mo and Zr atoms, respectively. The band alignment is more clearly seen in the schematic diagram and the zoomed-in view of the band structure on the same energy scale shown in (c). The horizontal dashed line indicates the Fermi energy.

III. RESULTS AND DISCUSSION

As shown in Fig. 2(a), the highest occupied orbital of the $\text{MoTe}_2/\text{ZrS}_2$ heterostructure is localized on the Mo atom (magenta), while the first orbital of the conduction band is mainly localized on the Zr atom (blue). Consequently, the valence band maximum (VBM) of the heterostructure is unambiguously attributed to the MoTe_2 layer and is highlighted in magenta in the band structure, while the conduction band minimum (CBM) is attributed to the ZrS_2 layer and indicated in blue. For the sake of convenience, we keep the same color coding throughout the rest of this paper and focus on the relevant bands in the band structure representations. The band structure shown in Figs. 2(b) and 2(c) clearly represents a broken-gap band alignment for the $\text{MoTe}_2/\text{ZrS}_2$ vdW heterostructure: The CBM drops below the VBM, while the Fermi level touches the CBM at point M and intersects the valence band close to point K of the Brillouin zone. Few studies have reported such a broken-gap situation [35–37]. To shed some light on the origin of the observed band alignment in the heterostructure, we address the isolated constituent monolayers. Shown in Fig. 3(a) are the electronic band structures of the pristine monolayers. MoTe_2 possesses a direct gap at the K point, while ZrS_2 is a semiconductor with an indirect Γ -to- M gap. Both the MoTe_2 monolayer and the ZrS_2 monolayer are semiconductors with a 1-eV gap in agreement with the reported PBE calculations [38–40], whereas the gap is closed in the $\text{MoTe}_2/\text{ZrS}_2$ vdW heterostructure shown in Fig. 2(c).

We explore in the following three potential scenarios that may govern the broken-gap band alignment of the

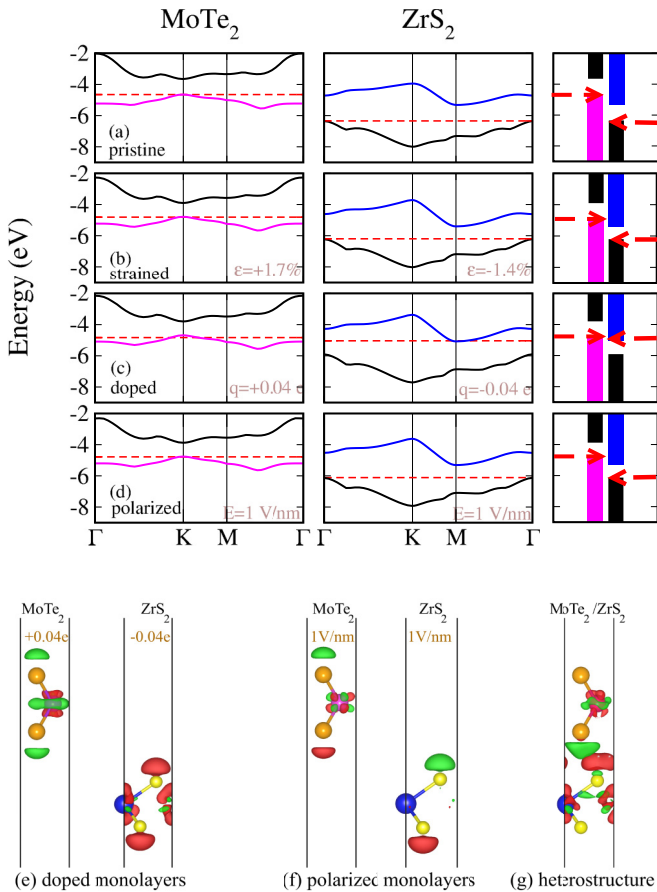


FIG. 3. Band structure of isolated monolayers of MoTe₂ and ZrS₂ (a) in pristine form, (b) subject to the same in-plane strain as in the heterostructure, (c) doped by the same net charge as in the heterostructure, or (d) subject to a normal-to-plane electric field as large as that produced by the interfacial dipole layer. The bands are aligned by reference to the vacuum level of the corresponding monolayer after eliminating the trivial contribution of the uniform external electric field or the homogeneous background charge to the electrostatic potential (see Supplemental Material [30]). The horizontal dashed lines indicate the Fermi energies, which approach a common value only for doped monolayers (c). Electron density difference maps show isosurfaces of $0.0002 e/\text{bohr}^3$ as induced by the doping (e) or polarizing electric field (f) corresponding to rows (b) and (c), respectively, or the formation of the heterostructure (g). Electron accumulation (depletion) is represented in red (green).

monolayers upon formation the vdW heterostructure: (i) the in-plane strain felt by each of the two layers due to their lattice mismatch, (ii) electric charge transfer from one layer to the other, and (iii) interfacial electric polarization. Although these three consequences of the formation of the heterostructure occur simultaneously, we address them separately to investigate their individual effects. To compare the band structure of the heterostructure with those of the pristine monolayers, shown in Figs. 2 and 3, respectively, we align the vacuum levels of the individual monolayers to a common reference so that the energies of their bands are comparable according to Anderson's rule [37]. A clear difference between the band structures of the heterostructure and the noninteracting pristine monolayers is the relative position of the CBM

and VBM while the Fermi energies of the isolated layers are still misaligned. (Recall that the VBM of the heterostructure has a MoTe₂ nature while the CBM originates from the ZrS₂ layer, hence the magenta-blue color coding.)

We first inspect the band structures of the isolated monolayers subject to the same strain felt in the heterostructure, i.e., $\epsilon = +1.7\%$ on MoTe₂ and -1.4% on ZrS₂, as illustrated in Fig. 3(b). The strained MoTe₂ and ZrS₂ layers remain gapped semiconductors with slightly reduced band gaps of 0.9 and 0.8 eV, respectively. Since no significant change is induced in the band structures, we rule out there being a role of the lattice-mismatch-induced strain in the closing of the gap in the heterostructure.

We next focus on the second scenario, i.e., charge transfer between the layers. The amount of the charge is estimated from the topology of the electron density based on the Bader charge analysis [41,42]. In this method, the real space is partitioned into a number of atomic basins in such a way that the electron density has a vanishing gradient (and is thus minimized) on the borders of the basins. In the present problem, we seek a hypothetical surface in the space that separates the MoTe₂ and ZrS₂ layers so that the volume integration of the electron density on each side of the surface gives the charge of the corresponding layer. The desired Bader surface is the locus of the electron density minimum between the two layers. Our charge analysis predicts that $0.04 e/f.u.$ is transferred from the MoTe₂ layer to the ZrS₂ layer upon formation of the MoTe₂/ZrS₂ vdW heterostructure. This tiny amount of charge transfer indicates that there is no chemical bonding between the atoms of opposite layers, but once injected into the semiconducting layers the resultant charge doping concentration is calculated to be $\sim 3.6 \times 10^{13} e/\text{cm}^2$, which is large enough to modify its conductivity [43]. For vertically stacked TFET applications, the MoTe₂ layer in the heterostructure may be understood as an *n*-type source, and the ZrS₂ layer may be understood as a *p*-type drain [10]. Now, to reveal the role of the charge transfer in the band alignment of the heterostructure, the band structure of the isolated layers doped by $q = \pm 0.04 e$ is presented in Fig. 3(c). Interestingly, the Fermi levels of the doped monolayers become aligned together. Moreover, the CBM of the negatively charged monolayer experiences a downshift and touches the common Fermi energy, while the VBM of the positively charged layer lies slightly above the Fermi energy. The band edge representation in the rightmost column in Fig. 3 helps the eye to better detect these changes. Overall, the overlap in Fig. 3(c) resembles the overlap in a broken-gap type of band alignment in the MoTe₂/ZrS₂ heterostructure; cf. Fig. 2(c). We thus attribute the broken-gap lineup in the MoTe₂/ZrS₂ heterostructure to the charge transfer between the layers.

Our Bader charge analysis reported above indicates that MoTe₂ donates electrons to ZrS₂ upon the formation of the heterostructure. The spatial distribution of the electron density difference, $\Delta n = n_{\text{ZrS}_2/\text{MoTe}_2} - (n_{\text{ZrS}_2} + n_{\text{MoTe}_2})$, illustrated in Fig. 3(g), clearly shows not only a charge redistribution around the Zr and Mo atoms (the doping scenario addressed above) but also a pronounced electron accumulation and depletion at the interface of the vdW heterostructure around the S and Te atoms, respectively. The resultant *interfacial electric dipole layer* develops an effectively normal-to-plane

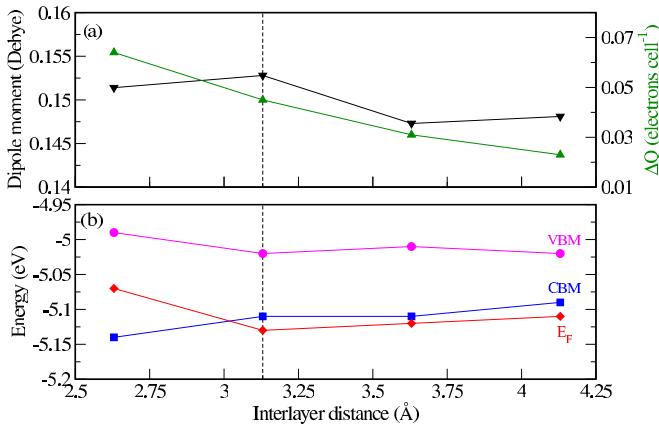


FIG. 4. Bader effective charge on each layer and total dipole moment of the cell (a) and Fermi, VBM, and CBM energies (b) of the $\text{MoTe}_2/\text{ZrS}_2$ vdW heterostructure as a function of the interlayer distance. The dashed vertical line indicates the position of the equilibrium interlayer distance.

electric field which points from ZrS_2 towards MoTe_2 . We therefore investigate, as the third scenario, the effect of this intrinsic interfacial polarization on the band alignment of the heterostructure. The band structure of the isolated pristine monolayers subject to such a normal-to-plane electric field of strength 1 V/nm is shown in Fig. 3(d) and reveals that the CBM of ZrS_2 still lies well below the VBM of MoTe_2 while the two Fermi levels are not aligned. Estimating the strength of the electric field developed by the interfacial dipole layer is not straightforward. Since an external electric field of strength 0.45 V/nm is required to compensate the intrinsic dipole moment of the heterostructure (see Fig. 5), the field developed by the interfacial dipole layer in the layers is assumed to have a similar magnitude [hence 1 V/nm in Fig. 3(d)]. However, we repeated the test for several field strengths from 0.1 to 5 V/nm and even inverted the field direction, but the desired alignment of the Fermi energies is not observed. We can thus confidently conclude that the responsible factor for the band alignment is solely the exchanged charge that is injected into the layers to sit on the TM atoms but not the interfacial charge sitting on the chalcogens. Correspondingly, as illustrated in Figs. 3(e) and 3(g), respectively, doping the isolated layers leads to the same charge localization on the Zr atom as in the heterostructure. In contrast, the spatial distribution of the electron density difference induced by a polarizing electric field in the isolated layers does not resemble Δn on the TM atoms in the heterostructure, as clearly seen in Figs. 3(f) and 3(g), respectively.

We finally investigate the robustness of the broken-gap band alignment of the heterostructure in the presence of a normal-to-plane tensile or compressive stress or electric field as reported in Figs. 4 and 5, respectively. While the Fermi level as well as the valence and conduction band edges have no significant change from their values at the equilibrium separation (i.e., 3.13 Å, indicated by a dashed line), the amount of transferred charge decreases monotonically with increasing interlayer separation. This implies that a charge transfer of 0.02 e is enough for the broken-gap band lineup. On the other hand, the band alignment is preserved also when a compres-

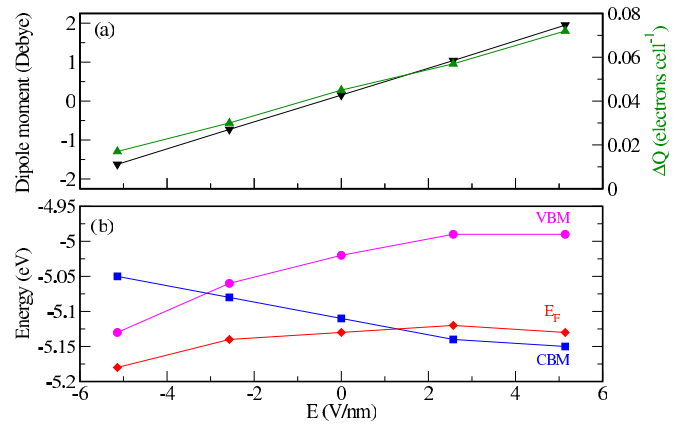


FIG. 5. (a) and (b) Same as Fig. 4, but for external electric field normal to the plane of the layers. A positive value of E in (b) corresponds to the direction from ZrS_2 to MoTe_2 .

sive strain is applied (by reducing the interlayer distance by 0.5 Å), but then the overlap of the valence and conduction bands even increases.

The effect of an external electric field perpendicular to the plane of the layers, corresponding to applying a gate voltage to the heterostructure, is shown in Fig. 5. The external field in the same direction as the intrinsic interfacial field (i.e., pointing from ZrS_2 to MoTe_2), increases both the interfacial dipole moment and the electron transfer from MoTe_2 to ZrS_2 but changes marginally the overlap between the valence and conduction bands. In fact, a small charge hosted by the central TM atoms already leads to a broken-gap band alignment, while increasing the transferred charge which is delocalized over the interface plays no significant role in the band alignment. On the other hand, an opposite field pointing from the MoTe_2 layer towards the ZrS_2 layer lifts up the CBM and pushes down the VBM, so that the overlap between the valence and conduction bands is reduced. (In fact, such an opposite field of magnitude 0.45 V/nm suppresses completely the heterostructure dipole moment and thus gives an estimation of the strength of the intrinsic electric field developed by the interfacial dipole layer, as mentioned above.) As long as the layers are charged, the broken-gap type of band alignment survives. This correlated behavior of the transferred charge and band alignment is independent of the interface polarization. Our Bader charge analysis reveals that the Zr atom hosts extra electrons even under a strong field that reverses the interfacial polarization. Eventually, once the field exceeds 2.7 V/nm (which is almost five times the field required to suppress the interfacial dipole moment) a staggered band lineup is observed. In short, the band overlapping of $\text{MoTe}_2/\text{ZrS}_2$ is a robust broken-gap band alignment and survives being subject to large normal-to-plane strains or strong electric fields. Moreover, since the heterostructure is formed mainly due to vdW interactions, one expects there to be no significant corrugations at the interface. Nevertheless, imperfections such as interface incoherency are translated into local interface polarization, charge transfer, in-plane strain, perpendicular strain, or local electric fields. We showed that the predicted broken-gap band alignment is robust against such basic factors

and expect that the explained mechanism remains valid for nonideal interfaces in real-world experiments.

IV. SUMMARY

To summarize, we studied the electronic properties of the $\text{MoTe}_2/\text{ZrS}_2$ vdW heterostructure using first-principles calculations. A robust, intrinsic broken-gap band alignment is observed which can hardly be switched to the staggered-gap band alignment. We introduced a methodology that involves breaking up the complex heterostructure into isolated monolayers. Comparing the relative positions of the band edges of the heterostructure with those of the isolated monolayers in different situations (pristine, charged, and subject to external strain or electric field), we explored three scenarios to uncover the origin of the band alignment. We found that despite the localization of the transferred charge upon formation of the heterostructure basically over the interface of the layers, the less-pronounced accumulation of electrons on the Zr atom

is responsible for the broken-gap alignment. The relative arrangement of the VBM and CBM in the heterostructure looks similar to the position of the VBM of a hole-doped MoTe_2 monolayer relative to the CBM of the electron-doped ZrS_2 monolayer while their Fermi energies are aligned. The charge state of Zr remains almost constant when applying an external normal-to-plane strain or electric field, resulting in a robust broken-gap type of band alignment. A transition to the more common staggered-gap band alignment requires applying an extremely strong inverse external electric field of a few V/nm, which is too large compared with the typical macroscopic dielectric strengths used to prevent dielectric breakdown. Our findings would be useful for the design and electronic structure tuning of the heterojunctions based on TMDs.

ACKNOWLEDGMENTS

S.S.A. acknowledges the Marconi supercomputing system based at CINECA, Italy. Computational resources were partially provided by the SARMAD cluster at SBU.

-
- [1] K. Liang, T. Huang, K. Yang, Y. Si, H.-Y. Wu, J.-C. Lian, W.-Q. Huang, W.-Y. Hu, and G.-F. Huang, Dipole Engineering of Two-Dimensional van der Waals Heterostructures for Enhanced Power-Conversion Efficiency: The Case of Janus $\text{Ga}_2\text{SeTe/InS}$, *Phys. Rev. Appl.* **16**, 054043 (2021).
- [2] H. Kroemer, Nobel Lecture: Quasielectric fields and band offsets: teaching electrons new tricks, *Rev. Mod. Phys.* **73**, 783 (2001).
- [3] P. Zereszki, P. Yao, D. He, Y. Wang, and H. Zhao, Interlayer charge transfer in ReS_2/WS_2 van der Waals heterostructures, *Phys. Rev. B* **99**, 195438 (2019).
- [4] L. Xiang, Q. Zhang, and Y. Ke, Strong interlayer excitons in $\text{PtSe}_2/\text{ZrS}_2$ van der Waals heterobilayer, *Appl. Phys. Lett.* **118**, 093101 (2021).
- [5] Y. Guo and J. Robertson, Band engineering in transition metal dichalcogenides: Stacked versus lateral heterostructures, *Appl. Phys. Lett.* **108**, 233104 (2016).
- [6] M. Cao, L. Luan, Z. Wang, Y. Zhang, Y. Yang, J. Liu, Y. Tian, X. Wei, J. Fan, Y. Xie, and L. Duan, Type-II GeC/ZnTe heterostructure with high-efficiency of photoelectrochemical water splitting, *Appl. Phys. Lett.* **119**, 083101 (2021).
- [7] Q. Li, K.-Q. Chen, and L.-M. Tang, Large Valley Splitting in van der Waals Heterostructures with Type-III Band Alignment, *Phys. Rev. Appl.* **13**, 014064 (2020).
- [8] P. K. Srivastava, Y. Hassan, Y. Gebredingle, J. Jung, B. Kang, W. J. Yoo, B. Singh, and C. Lee, Van der Waals broken-gap p-n heterojunction tunnel diode based on black phosphorus and rhenium disulfide, *ACS Appl. Mater. Interfaces* **11**, 8266 (2019).
- [9] C. Lei, Y. Ma, X. Xu, T. Zhang, B. Huang, and Y. Dai, Broken-gap type-III band alignment in $\text{WTe}_2/\text{HfS}_2$ van der Waals heterostructure, *J. Phys. Chem. C* **123**, 23089 (2019).
- [10] C. Gong, H. Zhang, W. Wang, L. Colombo, R. M. Wallace, and K. Cho, Band alignment of two-dimensional transition metal dichalcogenides: Application in tunnel field effect transistors, *Appl. Phys. Lett.* **103**, 053513 (2013).
- [11] Anh Khoa Augustin Lu, M. Houssa, M. Luisier, and G. Pourtois, Impact of Layer Alignment on the Behavior of $\text{MoS}_2\text{-ZrS}_2$ Tunnel Field-Effect Transistors: An *Ab Initio* Study, *Phys. Rev. Appl.* **8**, 034017 (2017).
- [12] X. Zhu, J. He, R. Zhang, C. Cong, Y. Zheng, H. Zhang, S. Zhang, and L. Chen, Effects of dielectric screening on the excitonic and critical points properties of WS_2/MoS_2 heterostructures, *Nanoscale* **12**, 23732 (2020).
- [13] T. Deilmann, F. Withers, J. Escolar, D. Nutting, T. Taniguchi, K. Watanabe, A. Taghizadeh, M. F. Craciun, K. S. Thygesen, and S. Russo, Electrical tuning of optically active interlayer excitons in bilayer MoS_2 , *Nat. Nanotechnol.* **16**, 888 (2021).
- [14] H.-P. Komsa and A. V. Krasheninnikov, Electronic structures and optical properties of realistic transition metal dichalcogenide heterostructures from first principles, *Phys. Rev. B* **88**, 085318 (2013).
- [15] N. A. Pike, A. Dewandre, F. Chaltin, L. Garcia Gonzalez, S. Pillitteri, T. Ratz, and M. J. Verstraete, Spontaneous interlayer compression in commensurately stacked van der Waals heterostructures, *Phys. Rev. B* **103**, 235307 (2021).
- [16] W. Wang, K. Li, Y. Wang, W. Jiang, X. Liu, and H. Qi, Investigation of the band alignment at $\text{MoS}_2/\text{PtSe}_2$ heterojunctions, *Appl. Phys. Lett.* **114**, 201601 (2019).
- [17] R. Rao, A. E. Islam, S. Singh, R. Berry, R. K. Kawakami, B. Maruyama, and J. Katoch, Spectroscopic evaluation of charge-transfer doping and strain in graphene/ MoS_2 heterostructures, *Phys. Rev. B* **99**, 195401 (2019).
- [18] X. Yang, X. Qin, J. Luo, N. Abbas, J. Tang, Y. Li, and K. Gu, $\text{HfS}_2/\text{MoTe}_2$ vdW heterostructure: bandstructure and strain engineering based on first-principles calculation, *RSC Adv.* **10**, 2615 (2020).
- [19] C. Xia, J. Du, M. Li, X. Li, X. Zhao, T. Wang, and J. Li, Effects of Electric Field on the Electronic Structures of Broken-gap Phosphorene/ SnX_2 ($X = \text{S}, \text{Se}$) van der Waals Heterojunctions, *Phys. Rev. Appl.* **10**, 054064 (2018).

- [20] P. Zereshki, P. Valencia-Acuna, and H. Zhao, All-optical control of charge transfer and interlayer excitons in transition metal dichalcogenide heterostructures, *Phys. Rev. B* **103**, 165416 (2021).
- [21] R. Liu, F. Wang, L. Liu, X. He, J. Chen, Y. Li, and T. Zhai, Band alignment engineering in two-dimensional transition metal dichalcogenide-based heterostructures for photodetectors, *Small Struct.* **2**, 2000136 (2021).
- [22] K. Nakamura, N. Nagamura, K. Ueno, T. Taniguchi, K. Watanabe, and K. Nagashio, All 2D heterostructure tunnel field-effect transistors: impact of band alignment and heterointerface quality, *ACS Appl. Mater. Interfaces* **12**, 51598 (2020).
- [23] H. Ilatikhameneh, Y. Tan, B. Novakovic, G. Klimeck, R. Rahman, and J. Appenzeller, Tunnel field-effect transistors in 2-D transition metal dichalcogenide materials, *IEEE J. Explor. Solid-State Comput. Devices Circuits* **1**, 12 (2015).
- [24] J. P. Perdew, K. Burke, and M. Ernzerhof, Generalized Gradient Approximation Made Simple, *Phys. Rev. Lett.* **77**, 3865 (1996).
- [25] P. Giannozzi, S. Baroni, N. Bonini, M. Calandra, R. Car, C. Cavazzoni, D. Ceresoli, G. L. Chiarotti, M. Cococcioni, I. Dabo, A. D. Corso, S. de Gironcoli, S. Fabris, G. Fratesi, R. Gebauer, U. Gerstmann, C. Gougoussis, A. Kokalj, M. Lazzeri, L. Martin-Samos *et al.*, QUANTUM ESPRESSO: A modular and open-source software project for quantum simulations of materials, *J. Phys.: Condens. Matter* **21**, 395502 (2009); P. Giannozzi, O. Andreussi, T. Brumme, O. Bunau, M. B. Nardelli, M. Calandra, R. Car, C. Cavazzoni, D. Ceresoli, M. Cococcioni, N. Colonna, I. Carnimeo, A. Dal Corso, S. de Gironcoli, P. Delugas, R. A. DiStasio, Jr., A. Ferretti, A. Floris, G. Fratesi, G. Fugallo *et al.*, Advanced capabilities for materials modelling with Quantum ESPRESSO, *ibid.* **29**, 465901 (2017); P. Giannozzi, O. Baseggio, P. Bonfá, D. Brunato, R. Car, I. Carnimeo, C. Cavazzoni, S. de Gironcoli, P. Delugas, F. Ferrari Ruffino, A. Ferretti, N. Marzari, I. Timrov, A. Urru, and S. Baroni, Quantum ESPRESSO toward the exascale, *J. Chem. Phys.* **152**, 154105 (2020).
- [26] D. R. Hamann, Optimized norm-conserving Vanderbilt pseudopotentials, *Phys. Rev. B* **88**, 085117 (2013).
- [27] L. Bengtsson, Dipole correction for surface supercell calculations, *Phys. Rev. B* **59**, 12301 (1999).
- [28] B. Meyer and D. Vanderbilt, *Ab initio* study of BaTiO₃ and PbTiO₃ surfaces in external electric fields, *Phys. Rev. B* **63**, 205426 (2001).
- [29] D. Cahen and A. Kahn, Electron energetics at surfaces and interfaces: concepts and experiments, *Adv. Mater.* **15**, 271 (2003).
- [30] See Supplemental Material at <http://link.aps.org/supplemental/10.1103/PhysRevB.106.245301> for the details of our numerical method for determining the vacuum levels of the pristine, charged, and polarized layers.
- [31] D. S. Koda, F. Bechstedt, M. Marques, and L. K. Teles, Coincidence lattices of 2D crystals: Heterostructure predictions and applications, *J. Phys. Chem. C* **120**, 10895 (2016).
- [32] S. Grimme, Semiempirical GGA-type density functional constructed with a long-range dispersion correction, *J. Comput. Chem.* **27**, 1787 (2006).
- [33] I. Hamada, van der Waals density functional made accurate, *Phys. Rev. B* **89**, 121103(R) (2014).
- [34] T. Björkman, Testing several recent van der Waals density functionals for layered structures, *J. Chem. Phys.* **141**, 074708 (2014).
- [35] F. A. Rasmussen and K. S. Thygesen, Computational 2D materials database: Electronic structure of transition-metal dichalcogenides and oxides, *J. Phys. Chem. C* **119**, 13169 (2015).
- [36] V. O. Özçelik, J. G. Azadani, C. Yang, S. J. Koester, and T. Low, Band alignment of two-dimensional semiconductors for designing heterostructures with momentum space matching, *Phys. Rev. B* **94**, 035125 (2016).
- [37] F. H. Davies, C. J. Price, N. T. Taylor, S. G. Davies, and S. P. Hepplestone, Band alignment of transition metal dichalcogenide heterostructures, *Phys. Rev. B* **103**, 045417 (2021).
- [38] H.-g. Kim and H. J. Choi, Thickness dependence of work function, ionization energy, and electron affinity of Mo and W dichalcogenides from DFT and GW calculations, *Phys. Rev. B* **103**, 085404 (2021).
- [39] K. W. Lau, C. Cocchi, and C. Draxl, Electronic and optical excitations of two-dimensional ZrS₂ and HfS₂ and their heterostructure, *Phys. Rev. Mater.* **3**, 074001 (2019).
- [40] O. Rubel, Kinetic mechanism for reversible structural transition in MoTe₂ induced by excess charge carriers, *Phys. Rev. B* **97**, 224101 (2018).
- [41] R. F. W. Bader, Atoms in molecules, *Acc. Chem. Res.* **18**, 9 (1985).
- [42] G. Henkelman, A. Arnaldsson, and H. Jónsson, A fast and robust algorithm for Bader decomposition of charge density, *Comput. Mater. Sci.* **36**, 354 (2006).
- [43] S. S. Ataei and A. Sadeghi, Competitive screening and band gap renormalization in *n*-type monolayer transition metal dichalcogenides, *Phys. Rev. B* **104**, 155301 (2021).